Unravelling the Crystallization Process in Solution-Derived $YBa_2Cu_3O_{7-\delta}$ Nanocomposite Films with Preformed ZrO_2 Nanocrystals via Definitive Screening Design

Hannes Rijckaert,* Pablo Cayado,* Jens Hänisch, Jonas Billet, Manuela Erbe, Bernhard Holzapfel, and Isabel Van Driessche

ABSTRACT: A low-cost chemical solution deposition technique was employed to prepare $YBa_2Cu_3O_{7-\delta}$ (YBCO) nanocomposite films starting from a colloidal solution containing preformed ZrO_2 nanocrystals. As previous publications revealed, an increase in the amount of nanocrystals results in a progressive deterioration of the film properties. The parameters that control this process and their interplay are still unknown in detail. Using definitive screening design (DSD), a design-of-experiments approach, allowed determining which of the multiple growth parameters play a key role for improving the superconducting properties of YBCO nanocomposite films even with a large concentration of nanocrystals. In order to show the potential of DSD, it has been applied for the optimization of two different properties: the critical temperature T_c and the full width at half-maximum of the (005) YBCO reflection. This work shows that DSD is a powerful and efficient method that allows optimizing certain processes with a minimal number of experiments.

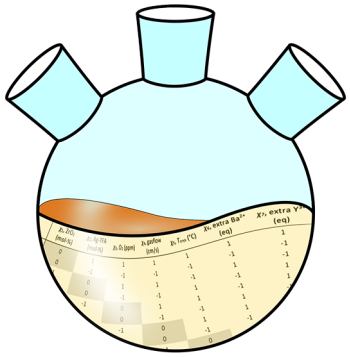

$REBa_2Cu_3O_{7-\delta}$ (REBCO, RE = rare earth) films are the functional materials of coated conductors (CCs), a combination of a flexible metallic substrate and a superconducting functional layer as well as several buffer and protection layers. CCs have the potential to offer a highly efficient and environmentally friendly extension of tomorrow's energy conversion, transport, and usage.[1] Therefore, the reliable and low-cost large-scale fabrication of REBCO films is essential for enabling the construction of superconductor-based electric power applications such as motors and generators with working conditions at 77 K and low magnetic field range (<1 T).[2] Nowadays, there are major obstacles for the successful implementation and distribution of CCs throughout the energy market. First, pristine REBCO films typically exhibit a strong reduction of critical current densities (J_c) in applied magnetic fields $B = \mu_0 H$ caused by vortex motion. Second, the highly anisotropic nature of the REBCO crystal structure with currents mainly flowing within the *ab*-oriented CuO_2 planes as well as the J_c-limiting nature of large-angle grain boundaries[3] (due to the extremely short coherence lengths) necessitates near-perfect biaxial textures for large current carrying capabilities.[4] In order to overcome these difficulties, it becomes crucial to immobilize (to pin) the vortices and thus to enhance J_c for all magnetic fields and orientations as well as to achieve a perfect biaxial texture to ensure a continuity of the CuO_2 planes and to avoid large-angle grain boundaries.

In recent decades, the incorporation of nanosized defects to the REBCO matrix has proved to be an effective approach to achieve the immobilization of vortices.[5−7] Many fabrication methods of REBCO and in particular of $YBa_2Cu_3O_{7-\delta}$ (YBCO) nanocomposite films have been reported.[8−11] Among them, chemical solution deposition (CSD) has the potential to be easily scalable with reduced cost compared to vacuum deposition methods. In this work, the cost-effective CSD technique starting from colloidalYBCO solutions was used.[12] This so-called *ex-situ* approach (i.e., preformed nanocrystals in YBCO solutions) faces some challenges like the limitation of the nanocrystal amount that can be introduced without decreasing the superconducting properties.[13] This phenomenon has been related to Ba^{2+} consumption of the metal oxide nanocrystals (e.g., HfO_2, ZrO_2, and CeO_2) during the YBCO growth, leading to a poorer YBCO texture.[14,15]

Although the optimization of the growth of these nanocomposite films has been investigated in depth in the last years, all related reports reveal great effort and difficulties to achieve

better performance in this type of films. Investigations at the lab scale via common experiments where one processing parameter at the time is studied, imply a large number of experiments due to the multitude of potentially important parameters. In order to optimize the resources and to decrease the effort (both in time and money) spent in these investigations, combinatorial approaches have emerged as an interesting option that allow to accelerate the research and development process through parallel and rapid sequential experimentation.[16] The continuous composition spread (CCS) approach has already been applied for film deposition of oxide materials via pulsed laser deposition and sputtering.[17−19] The CCS approach has the advantage of being able to grow thin-films with several dozens of compositions at a time compared with conventional solid-state synthesis. However, this approach is not possible for CSD YBCO nanocomposites due to the complexity of CSD.[12] Definitive screening design (DSD), which is applied to CSD-based YBCO nanocomposites for the first time, is a powerful screening method to estimate the model coefficients of the main effects, two-factor interactions, and quadratic effects for k factors with only a minimal number of experiments.[20−22] It has been used previously to study the growth of pristine REBCO films by Hayasaka et al.[23] for the case of ErBCO films.

The objective of this work was to use DSD to investigate and determine the synthesis parameters that have a significant impact on the final properties, which in the end will lead to the optimization of YBCO *ex-situ* nanocomposite properties without having to perform an unreasonably high number of experiments. In addition, the DSD approach helps to clarify the effect and interplay of the synthesis parameters that control the microstructure and/or superconducting properties of CSD-YBCO nanocomposite films and therefore to obtain high-quality films with a higher amount of preformed metal oxide nanocrystals. It is very important to consider the way in which DSD works. DSD usually focuses on the optimization of a single property without considering others. Therefore, the obtained optimized parameters for one property could be very different from the ones obtained for a different property and can even show opposing trends. This means that one should select the most adequate property for a certain application or purpose because the rest of the properties may not follow the same trend and can even have deteriorated.

In our case, in order to improve the properties of the films, the first requirement is to design a suitable growth process that allows obtaining epitaxial, *c*-axis oriented films. There are different strategies to improve the growth process to achieve that process: (1) adding silver to stabilize the *c*-axis nuclei,[24] (2) adjusting the stoichiometric ratio of Y:Ba:Cu in the YBCO precursor solution,[25,26] (3) introducing a pristine YBCO seed layer to ensure *c*-axis growth of the YBCO nanocomposite,[13] and (4) modifying the crystallization process. Applying DSD for these four points, we achieved YBCO nanocomposite films with larger amounts of ZrO_2 nanocrystal than had been possible before (up to 12.5 mol %) without damaging yet even improving the YBCO microstructure and the superconducting properties of the films. Therefore, this work shows that the derived DSD model is able to optimize the growth conditions regarding a certain property. The introduction of DSD in CSD can be a reference for further projects in the fabrication of functional thin films in several material classes, including multiferroics,[27] ferromagnetics,[27] ferroelectrics,[28] and piezoelectrics.[29]

EXPERIMENTAL SECTION

ZrO_2 Nanocrystals. These nanocrystals were synthesized and purified according to De Keukeleere et al.[30] $Zr(OiPr)_4{\cdot}iPrOH$ (1.55 g, 4 mmol), $ZrCl_4$ (1.166 g, 5 mmol), and 20 g tri-*n*-octylphosphine oxide were mixed, and the temperature of this mixture was raised to 340 °C. The synthesis was carried out in an argon atmosphere and under vigorous stirring for 2 h. After the heating-up synthesis, the nanocrystals were purified by the addition of acetone (1:4 in volume) to the reaction mixture, which resulted in a white precipitate after centrifugation at a relative centrifugal force of 4508 *g* for 2 min. The precipitate was redispersed in methanol via the addition of a phosphonate-containing copolymer, which lead to a transparent and stable ZrO_2 nanosuspension (concentration of 0.3 M) with a solvodynamic diameter of 5.9 ± 1.9 nm, as confirmed via dynamic light scattering measurements described in the literature.[31]

Chemical Solution Deposition of YBCO Nanocomposite Films. The YBCO precursor solution was prepared by dissolving $Y(C_3H_5O_2)_3$, $Ba(CF_3CO_2)_2$, and $Cu(C_3H_5O_2)_2$ in methanol with a Y:Ba:Cu stoichiometric ratio of 1:2:3. The ZrO_2 nanosuspension was added to the YBCO precursor solution with the desired molar percentage of ZrO_2 nanocrystals (0, 2.5, 7.5, or 12.5 mol %) and adjusted to the total YBCO concentration (sum of salts) of 1.08 mol L^{-1}. The (100)-oriented $LaAlO_3$ single crystal substrates were supplied by a single manufacturer (CrysTec GmbH) to ensure their quality varies only insignificantly from substrate to substrate. These $LaAlO_3$ substrates were chemically and thermally treated in order to remove impurities and to reconstruct the surface termination as described in the literature.[32] Furthermore, they were cleaned with 2-propanol and heated to 400 °C to improve their wettability. First, an interfacial seed layer was prepared by depositing a more diluted pristine YBCO solution (0.24 mol L^{-1}) on the $LaAlO_3$ substrates by spin-coating (2000 rpm for 1 min) and pyrolyzing it before the deposition of the nanocomposite layer. The final thickness of this seed layer after all heat treatments was around 45 nm. Second, a standard YBCO thin film processing[33] was used: the YBCO solution was deposited by spin-coating (2000 rpm for 1 min) on $LaAlO_3$ substrates with pyrolyzed seed layer and subsequently dried at 65 °C on a hot plate in ambient atmosphere for 5 min. The dried films were pyrolyzed under humidified O_2 atmosphere with the heating ramps of 3 K min^{-1} from 25 to 195 °C, 0.1 K min^{-1} to 240 °C, and 5 K min^{-1} to a final temperature of 400 °C. The pyrolyzed films were subsequently crystallized by heating them to 815 °C with a rate of 5.5 °C min^{-1} and keeping this temperature for 45 min in a humid atmosphere of 200 ppm of O_2 in N_2. The inlet gas was bubbled through a water bath with a temperature of 23 °C and a gas flow of 3 cm s^{-1}. After the crystallization, the films were oxygenated in dry O_2 flow (1 atm) at 450 °C for 2 h in order to convert the tetragonal $YBa_2Cu_3O_6$ phase into the superconducting, orthorhombic $YBa_2Cu_3O_7$ phase. $AgCF_3CO_2$ (Ag-TFA) in a molar percentage of 3 or 6 mol % was added in some pristine seed layers as indicated in Tables 1 and 2, *cf* ref 24.

Microstructural and Electrical Characterization. Microstructure and phase purity of the films were investigated by X-ray diffraction (XRD) using a *Bruker* D8 diffractometer with Cu Kα radiation in Bragg−Brentano geometry. Self-field J_c at 77 K, J_c^{sf}, and critical temperature T_c were measured inductively with

Table 1. Seven Factors and Corresponding Factor Levels for the DSD Approach: the Concentration of ZrO_2 Nanocrystals (χ_1), the Mole Percentage of Ag-TFA in the YBCO Seed Layer (χ_2), the Oxygen Partial Pressure during the Crystallization (χ_3), The Gas flow during the Crystallization (χ_4), the Crystallization Temperature (χ_5), and the Addition of Extra Ba^{2+} (χ_6) and Extra Y^{3+} (χ_7)

factor	minimum	center	maximum
χ_1, ZrO_2 (mol %)	2.5	7.5	12.5
χ_2, Ag-TFA (mol %)	0	3	6
χ_3, O_2 (ppm)	100	300	500
χ_4, gas flow (cm s^{-1})	1	3	5
χ_5, T_{crys} (°C)	790	815	840
χ_6, extra Ba^{2+} (mol)	0	0.1	0.2
χ_7, extra Y^{3+} (mol)	0	0.15	0.30

a Cryoscan (*THEVA*, 50 μV criterion) and with a mutual-inductance method, respectively. T_c was defined as the value at 50% transition and the transition width as difference between the 10% and 90% values. Critical transport currents were measured in a 14-T Quantum Design Physical Property Measurement System in maximum Lorentz force configuration at 77 K with an electrical field criterion of 1 μV cm^{-1} on bridges of 800 μm length and 50 μm width prepared by wet chemical etching.

DSD Experiments. In order to identify the governing synthesis parameters ("factors" in DSD) for improving the superconducting properties of YBCO with higher content of nanocrystals, a DSD approach was introduced to monitor the so-called "responses" (Y), i.e., the resulting material properties, here T_c and the full width at half-maximum (fwhm) of the YBCO (005) reflections ($2\theta \sim 38.5°$). Seven factors (χ) had been identified as potentially affecting T_c and fwhm of YBCO (005): the concentration of ZrO_2 nanocrystals (χ_1), the mole percentage of Ag-TFA in the YBCO seed layer (χ_2), the oxygen partial pressure during the crystallization (χ_3), the gas flow during the crystallization (χ_4), and the crystallization temperature (χ_5) as well as excess Ba^{2+}, β (χ_6), and excess Y^{3+}, α (χ_7), in the formula unit $Y_{1+\alpha}Ba_{2+\beta}Cu_3O_{7-\delta}$. The concentration of the YBCO precursor solution, $LaAlO_3$ substrate, deposition and pyrolysis procedure were kept unchanged. DSD are constructed using conference matrices, which only work for an even number of factors k. When k is odd, a $(k + 1) \times (k + 1)$ conference matrix is used, of which the last column (dummy factor $k + 1$) is deleted.[20] With a center run added, a seven-factor ($k = 7$) design requires a minimum set of $2k + 3 = 17$ "trainings", i.e., single experiments, to identify the factors causing a significant nonlinear effect. The general structure of the design matrix consists of k foldover pairs with a center value (marked with gray in Table 2) in each column, two extra runs, and a center run. Adding the center run in the last row of the design matrix enables the model to include an intercept and all main and quadratic effects. Extra runs are constructed using dummy factors in the design matrix, improving its ability to identify active second-order effects.[21] DSD estimates main effects, two-factor interaction effects, and quadratic effects. An interaction effect is the simultaneous effect of two independent variables on at least one dependent variable, in which their joint effect is significantly greater than the sum of the parts.[34] The quadratic effects describe an optimum, which means that the "optimum" factor levels are not at the boundaries of the experimental region, but somewhere in between.[22]

The parameter values (minimum, center, and maximum) shown in Table 1 had been chosen based on previous work[35] and literature study. In preliminary experiments under similar conditions, the responses for pristine and 5 mol % ZrO_2 added

Table 2. Training Sets of Definitive Screening Design with Seven Factors: the Concentration of ZrO_2 Nanocrystals (χ_1), the Mole Percentage of Ag-TFA in the YBCO Seed Layer (χ_2), the Oxygen Partial Pressure during the Crystallization (χ_3), the Gas Flow during the Crystallization (χ_4), the Crystallization Temperature (χ_5), the Addition of Extra Ba^{2+} (χ_6) and extra Y^{3+} (χ_7), and the Obtained Critical Temperature (T_c), Critical Current Densities (J_c), and FWHM of YBCO (005) as Responses[a]

	parameters							responses			
	χ_1, ZrO_2 (mol %)	χ_2, Ag-TFA (mol %)	χ_3, O_2 (ppm)	χ_4, gas flow (cm s^{-1})	χ_5, T_{crys} (°C)	χ_6, extra Ba^{2+} (mol)	χ_7, extra Y^{3+} (mol)	T_c (K)	ΔT (K)	J_c(77 K) (MA cm^{-2})	fwhm YBCO (005)
T1	7.5	6	500	5	840	0.2	0.3	90.95	1.60	1.29	0.176(5)
T2	7.5	0	100	1	790	0	0	90.80	1.20	2.41	0.194(4)
T3	12.5	3	500	5	790	0.2	0	91.75	0.60	2.22	0.195(2)
T4	2.5	3	100	1	840	0	0.3	–	–	–	0.299(2)
T5	12.5	0	*300*	5	840	0	0.3	90.90	0.80	3.21	**0.164(1)**
T6	2.5	6	*300*	1	790	0.2	0	**92.55**	0.85	**3.67**	**0.162(1)**
T7	12.5	0	100	3	840	0.2	0	83.40	5.30	–	0.259(5)
T8	2.5	6	500	3	790	0	0.3	91.15	1.90	2.10	0.177(2)
T9	12.5	6	100	1	*815*	0.2	0.3	88.25	3.35	0.60	0.219(1)
T10	2.5	0	500	5	*815*	0	0	88.40	3.50	0.84	0.192(5)
T11	12.5	0	500	1	790	*0.1*	0.3	90.30	3.90	1.34	0.187(2)
T12	2.5	6	100	5	840	*0.1*	0	–	–	–	0.274(3)
T13	12.5	6	100	5	790	0	*0.15*	88.00	2.45	0.99	0.245(1)
T14	2.5	0	500	1	840	0.2	*0.15*	91.75	**0.55**	3.25	**0.159(2)**
T15	12.5	6	500	1	840	0	0	**93.15**	1.20	**3.99**	0.176(3)
T16	2.5	0	100	5	790	0.2	0.3	82.10	4.80	–	0.240(1)
T17	7.5	3	*300*	3	*815*	*0.1*	*0.15*	90.30	0.90	2.96	0.165(1)

[a]The amount of extra Ba^{2+}, β, and Y^{3+}, α, relates to the formula $Y_{1+\alpha}Ba_{2+\beta}Cu_3O_{7-\delta}$. Numbers in parentheses show the error of fwhm in the last digit. Some of the best values of T_c, ΔT, J_c and fwhm are highlighted in bold, illustrating that high J_c values often concur with high T_c values and/or low fwhm values. Center values in the design matrix are marked with italics.

nanocomposite YBCO films show similar outcomes for fwhm, J_c, and T_c with insignificant variances. Therefore, the extra center runs to estimate the population variance of responses as described by Hayasaka et al.[23] were not included in the training set. For the analysis of the responses, the statistical software package JMP was used. The p-value (see Table 3) is

Table 3. Coefficients of the Significant Main and Interaction Effects for the T_c Model with the Respective p-Values

factor	coefficient	p-values
χ_1, ZrO_2 (mol %)	0.388	0.48406
χ_3, O_2 (ppm)	2.185	0.00265
χ_4, gas flow (cm/s)	−1.573	0.01489
χ_6, extra Ba^{2+}(eq)	−0.890	0.04365
χ_1, ZrO_2(mol %) and χ_4, gas flow (cm/s)	1.681	0.01687

the tail probability in the standard t-distribution curve. It is computed by integrating the standard t-distribution function from t to infinity.[20] A p-value <0.05 indicates by definition a significant effect. The model selection is done by minimizing the corrected Akaike Information Criterion (AICc).[36] The AICc finds the optimum in the trade-off between the goodness of fit and the model's simplicity. This way, the risk of either over- or underfitting is minimized.

In order to show the usefulness of the DSD approach, the models for the dependencies of two different properties were obtained and compared. T_c and the fwhm of the (005) YBCO reflection in $\theta-2\theta$ scans were selected as target properties due to their simplicity and because they are fast and easy to obtain and at the same time very useful for our purpose of demonstrating on the usefulness of DSD. Both properties are of vital importance for optimizing the film properties. On the one hand, T_c yields information on the compositional homogeneity of the films and is related with the oxygen content of the films. Even though J_c (especially in applied magnetic fields) and T_c are not strictly correlated, an adequately high T_c value is a necessary although not sufficient condition for high current carrying capabilities. On the other hand, the fwhm of the (005) YBCO reflection is related with the crystallinity of the films in such a way that the lower the fwhm (i.e., the sharper the reflection), the larger is the crystallinity of the YBCO matrix in the nanocomposite films. This again has a positive effect on the stiffness of the superconducting phase, i.e., the Cooper pair density and therefore the pinning potential as well as J_c, especially under self-field conditions. Both properties are therefore very relevant and interesting to optimize. The results of the 17 experiments of the training set (samples "T") are shown in Table 2.

$$T_c = 89.296 + 0.388\left(\frac{\chi_1 - 7.5}{5}\right) + 2.185\left(\frac{\chi_3 - 300}{200}\right) - 1.573\left(\frac{\chi_4 - 3}{2}\right) - 0.890\left(\frac{\chi_6 - 0.1}{0.1}\right) + 1.681\left(\frac{\chi_1 - 7.5}{5}\right)\left(\frac{\chi_4 - 3}{2}\right) \quad (1)$$

The obtained T_c data set, Table 2, was analyzed regarding the significant effects (main−interaction−quadratic), and the optimum model according to the aforementioned AICc minimization is shown in Table 3 and eq 1. Two experiments showed no T_c values above 77 K; nevertheless, they yielded important information on the possible growth conditions for superconducting YBCO nanocomposite films. Due to the very long duration of the oxygenation step (2 h at 450 °C in 1 atm O_2 flow) of these rather thin films (~350 nm),[37] this step is expected to allow for a complete oxygenation of the superconducting matrix. Hence, T_c must be determined by other parameters, i.e., the crystallization process. These films were grown with a combination of a low oxygen partial pressure of 100 ppm with a high crystallization temperature of 840 °C, which lies below the stability line of the YBCO phase in the oxygen partial pressure vs temperature diagram as described in the literature.[38,39] Those values clearly are not an option for producing high-quality superconducting YBCO nanocomposite films. These data had to be excluded when compiling the data in the model. The synthesis parameters that led to such low T_c values are far away from optimum growth parameters of YBCO. Therefore, these low T_c values are related with a bad crystalline quality of the films due to a wrong growth process and, again, not to the oxygenation process.

Three main factors were identified as having a significant influence ($p < 0.05$) on the T_c response in the chosen parameter limits: the oxygen partial pressure during the crystallization (χ_3), the gas flow during the crystallization (χ_4), and the excess Ba^{2+} (χ_6). Furthermore, one two-factor interaction effect, namely between the concentration of ZrO_2 nanocrystals (χ_1) and the gas flow during the crystallization (χ_4), was observed. Their correlation indicates that the gas flow during the crystallization should be increased when the concentration of ZrO_2 nanocrystals is increased, which indicates kinetic reasons for the deterioration of *ex-situ* nanocomposites grown under conditions optimized for pristine films.[15] The concentration of ZrO_2 nanocrystals (χ_1), the mole percentage of Ag-TFA in the YBCO seed layer (χ_2), the crystallization temperature (χ_5), and extra Y^{3+} (χ_7) showed no significant influence on T_c ($p > 0.05$). Surprisingly, T_c does not significantly depend on the crystallization temperature, which seems to contradict multiple publications;[24,37] however, it does support the results of ref 40. Our conclusion is that, of course, T_c will depend on the crystallization temperature, but not in the studied range, between 790 and 840 °C, where other parameters play a more important role. T_c is expected to suffer a severe deterioration if this temperature is decreased far below 790 °C, where atomic ordering is slowed, or increased far above 840 °C, where secondary phase formation becomes considerable leading to a nonuniform cation depletion of the YBCO phase. As long as the phase is stable and well ordered, though, T_c is mainly determined by the following oxygenation process. T_c values of the YBCO films in this work, however, are not subject to the severe variation caused by the crystallization temperature since the studied temperature range is rather narrow. The coefficient for the excess Ba^{2+} (χ_6) is negative, which means T_c decreases with increasing Ba^{2+} addition. Since this is expected from literature on the effects of Ba off-stoichiometry, it supports the validity of the presented T_c model: Despite the nominal formula $Y_{1+\alpha}Ba_{2+\beta}Cu_3O_{7-\delta}$ with only positive values of β, the Ba stoichiometry of the matrix in our final YBCO films ranges from Ba-deficient, caused by Ba-consumption through the ZrO_2 nanocrystals,[15] to Ba-rich due to the Ba addition (χ_6). Therefore, it ranges from $Y_{1+\alpha}Ba_{1.88}Cu_3O_{7-\delta}$ (for $\chi_1 = 12.5$ and $\chi_6 = 0$ and assuming a complete conversion of ZrO_2 to $BaZrO_3$ nanocrystals) to $Y_{1+\alpha}Ba_{2.18}Cu_3O_{7-\delta}$ (for $\chi_1 = 2.5$ and $\chi_6 = 0.2$) and corresponds

to a decrease of T_c of roughly 2 K based on our T_c model. This coincides with the observations in the literature.[41] As mentioned in further literature reports,[42−44] a YBCO precursor solution with a slight barium deficiency can lead to a higher J_c and still maintain good T_c. The findings in these publications and in our T_c model are consistent with our previous work,[15] where the Ba^{2+} deficiency caused by Ba^{2+} consumption of ZrO_2 nanocrystals resulted in a delay rather than in a degradation of the YBCO nucleation and growth. In Figure 1, the

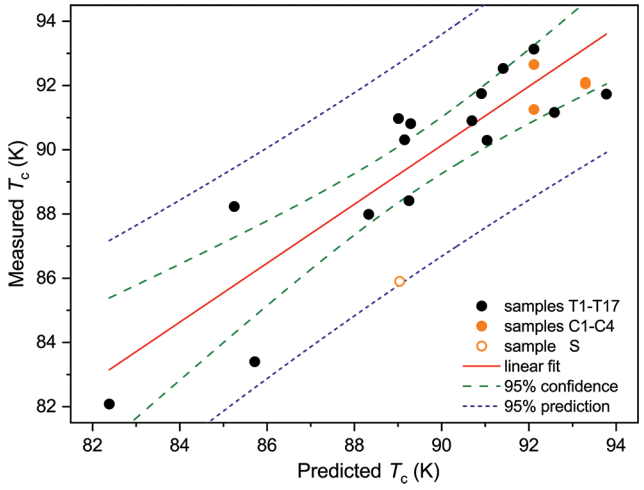

Figure 1. Measured T_c versus the predicted T_c according to the model, eq 1, for test samples T1−T17, Table 2, control samples C1−C4, and a "standard" sample S, Table 5. Samples T4 and T12 were omitted. Red full line: linear regression $y = mx + n$ with two fitting parameters slope $m = 0.92 \pm 0.14$ and intercept $n = 8 \pm 12$ K and R^2 of 0.78 and the RMSE of 2.07 K, including a 95% confidence band (green dashed line) and a 95% prediction band (blue dotted line). The fit function equals identity within error bars.

experimental T_c is plotted against the T_c values predicted by the model. The regression analysis with a linear fit shows a coefficient of determination (R^2) of 0.78 and a root mean square error (RMSE) of 2.07 K and indicates a good compliance between theoretical and experimental values while overfitting is avoided.

The analysis of the (005) fwhm values led to the significant effects and model presented below in Table 4 and eq 2. Figure

Table 4. Coefficients of the Significant Main, Interaction, and Quadratic Effects for the Model with Their Respective *p*-Values for FWHM YBCO (005) Values

factor	coefficient	*p*-values
χ_3, O_2 (ppm)	−0.0335	0.00002
χ_5, T_{crys} (°C)	0.0077	0.14060
χ_3, O_2 (ppm) and χ_5, T_{crys} (°C)	−0.0168	0.00746
χ_3, O_2 (ppm) and χ_3, O_2 (ppm)	0.0502	0.00096

2A displays a plot of the measured fwhm vs the predicted fwhm according to the fwhm model, eq 2, which has an R^2 value of 0.87 and an RMSE of 0.0002°. This indicates a better predictability of the fwhm compared to T_c and J_c, which is most likely at least partly due to the missing data points in the two latter cases. Similar to T_c, the effect of the oxygen partial pressure (χ_3) is significant, inferred by the low *p*-value. The oxygen partial pressure (χ_3) has even a quadratic effect on the fwhm, and thus the optimized parameter is found around the factor level "0", i.e., near 300 ppm. The other parameters with significant impact in the previous T_c case, on the other hand, are not significant here. In the fwhm model, the crystallization temperature (χ_5) is a factor of interest because of the significant interaction effect with the oxygen partial pressure (χ_3), Figure 2B. This is in accordance with the literature since the increase of crystallization temperature in the growth of YBCO is related with an improvement of the texture quality,[1,45] and unlike the previous case of T_c, the change between 790 and 840 °C makes a clear difference in the crystallinity of the films. As described in ref 24, the addition of Ag can help to enhance the stability of *c*-axis nucleation at the film/substrate interface during the crystallization process, ensuring the growth of a highly epitaxial crystalline YBCO film. However, both fwhm and the T_c model reveal that the presence of Ag in the seed layer (χ_2) shows no significant importance.

$$\text{FWHM} = 0.1634 - 0.0335\left(\frac{\chi_3 - 300}{200}\right) + 0.0502\left(\frac{\chi_3 - 300}{200}\right)^2 + 0.0077\left(\frac{\chi_5 - 820}{30}\right) - 0.0168\left(\frac{\chi_5 - 820}{30}\right)\left(\frac{\chi_3 - 300}{200}\right) \quad (2)$$

The two models discussed above are clearly distinctly different. Whereas the fwhm is only determined by the two parameters, O_2 pressure and T_{crys}, T_c needs to also take care of the gas flow, extra Ba^{2+}, and the amount of ZrO_2 besides the O_2 pressure, whereas the influence of T_{crys} is insignificant there. It should be noted that DSD, as applied here, focuses on the improvement of an individual property without necessarily considering others. This means that if one property is being optimized, it may happen—and as shown does—that others deteriorate. However, that is the nature of the DSD approach and material chemistry in general.

Presumably, also other important film characterizations, such as $J_c(sf, 77\ K)$, will depend on the oxygen partial pressure as do both T_c and the fwhm as stated by the low *p*-values of the main effect of χ_3 in both models as well as the quadratic effect in the fwhm model. Other properties, e.g., related to pinning, may show entirely different correlations, though, and even be independent of O_2 in the gas flow. We have shown two different models for the two investigated properties, showing how important it is to choose the right property for the optimization, because the resulting parameters will be unique for this particular property. In order to prove that DSD provides reliable models, we have selected the T_c model to conduct four control experiments (C1−C4 in Table 5) of nanocomposite films containing 12.5 mol %. ZrO_2 nanocrystals. This amount of ZrO_2 nanocrystals was chosen because growing a crystalline YBCO film with such a high amount of preformed ZrO_2 nanocrystals is a challenge. The gas flow (χ_4) and the stoichiometric ratio of Y:Ba:Cu (χ_6, χ_7) were set to 1 cm s^{-1} and 1:2:3, while the addition of Ag in the seed layer (χ_2) was avoided due to its low significance for T_c. A Monte Carlo simulation for the T_c model was conducted via JMP prediction profiler to determine the operating conditions necessary to grow such a YBCO nanocomposite with optimum T_c. An oxygen partial pressure of 500−600 ppm was chosen via prediction profiler in combination with the crystallization

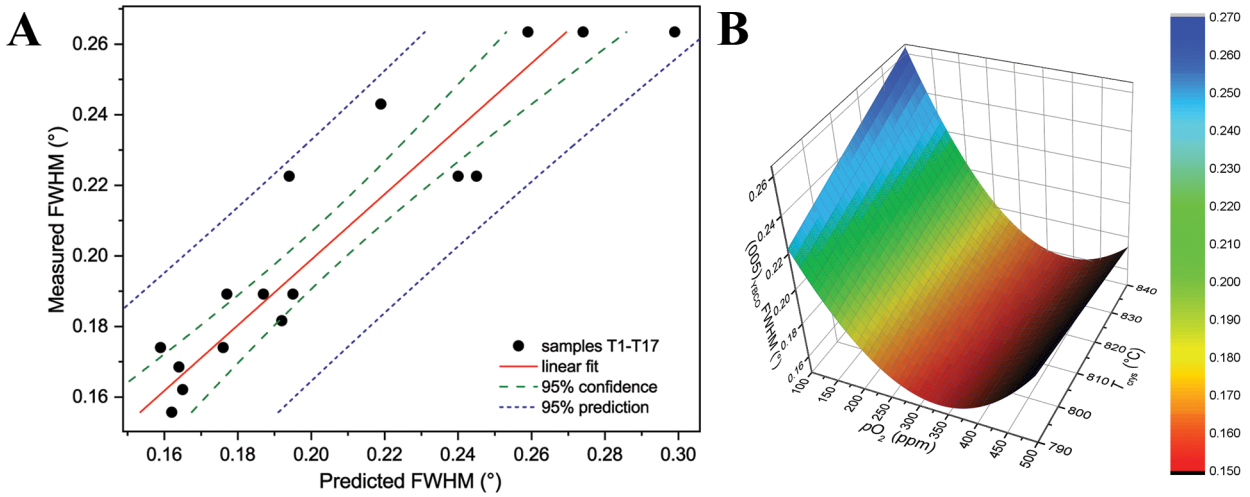

Figure 2. (A) Measured fwhm of (005) YBCO vs the predicted fwhm of (005) YBCO according to the model, eq 2, for test samples T1−T17, Table 2. Red full line: linear regression $y = mx + n$ with two fitting parameters slope $m = 1.07 \pm 0.10$ and intercept $n = 0.01 \pm 0.02$, an R^2 of 0.87, and the RMSE of 0.0002°, including 95% confidence band (green dashed line) and 95% prediction band (blue dotted line). The fit function equals identity within error bars. (B) 3D plot showing the behavior of fwhm of (005) YBCO over χ_3 (p_{O_2}) and χ_5 (T_{crys}).

Table 5. Control Experiments (C1−C4) and Experiment under Standard Conditions (S) with a Y:Ba:Cu Stoichiometric Ratio of 1:2:3, 12.5 mol % ZrO_2 Nanocrystals, and a Pristine Seed Layer without the Addition of Ag-TFA to Validate the T_c Model

	Parameters			*Responses*		
sample	χ_3, O_2 (ppm)	χ_4, gas flow (cm s^{-1})	χ_5,T_{crys} (°C)	T_c (K)	ΔT (K)	J_c(77 K) (MA cm^{-2})
C1	500	1	820	91.25	0.60	2.27
C2	500	1	840	92.65	0.45	3.72
C3	600	1	820	92.10	0.65	6.40
C4	600	1	840	92.05	1.35	1.30
S	200	3	815	85.90	6.80	–

temperature of 820−840 °C. The obtained T_c values, samples C1−C4 in Table 5, imply a remarkable improvement for T_c of YBCO + 12.5 mol % ZrO_2 with respect to such films grown under standard conditions of 200 ppm of O_2 with a gas flow of 1 cm s^{-1} at the crystallization temperature of 815 °C as described in ref 15 (sample "S" in Table 5). It is noteworthy that sample C3 even surpasses the best sample in ref 15 with a much lower ZrO_2 concentration of 5 mol % (T_c = 91.6 K, J_c = 5.8 MA cm^{-2}), for which such a DSD optimization was not done.

The pristine YBCO film and the above-mentioned YBCO+5 mol % ZrO_2 film grown under standard conditions described in ref 15 are compared with sample C3. Transport $J_c(B)$ of these three films (Figure 3) were measured at 77 K and normalized to the self-field J_c to show the trend of the performance of vortex pinning. Clearly, the addition of more nanocrystals leads to a smoother decay of the critical current density with increasing magnetic field and thus to a better performance. This result of increased flux pinning by increasing the amount of ZrO_2 nanoparticles was only possible by optimizing T_c toward the values of the samples with lower amount of nanoparticles, which shows that the DSD approach is a very valuable tool for the optimization of superconducting nanocomposite films with a large amount of preformed ZrO_2 nanocrystals. With this knowledge, the next step is to build new DSD experiments to optimize the amount of nanoparticles

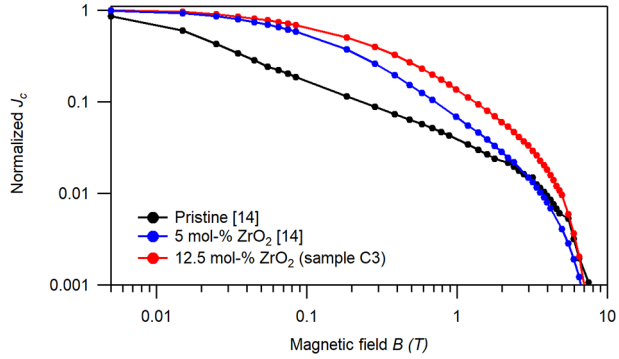

Figure 3. Comparison of the magnetic field dependence of transport J_c normalized to the self-field J_c at 77 K for YBCO films with different amounts of ZrO_2 nanocrystals. All samples had a comparable T_c of around 92 K.

for a certain range of temperature and magnetic field as well as to study other internal properties such as nanocomposite film thickness and the kind of the nanocrystals in the YBCO matrix.

For the first time, we employed a design of experiment method, namely the definitive screening design (DSD), to investigate the synthesis parameters that control the microstructural and superconducting properties of CSD-YBCO nanocomposite films. By performing a design of experiment with T_c and fwhm models, we showed that the main parameter for improving both YBCO crystallinity and T_c is the oxygen partial pressure as it has the most significant influence (lowest p-value). The T_c model refines the results of our previous work where the addition of ZrO_2 nanocrystals resulted in a delay of YBCO growth due to Ba^{2+} deficiency, which, as we concluded there, can be further optimized via tailoring the processing parameters during the crystallization. The fwhm model reveals that the oxygen partial pressure can improve the crystallinity of the YBCO matrix in the nanocomposite film. These observations are confirmed by the growth of YBCO nanocomposite films with a very high amount of ZrO_2 nanocrystals that previously led to poor superconducting properties. On the basis of the prediction of our DSD model, we were able to grow such films with outstanding, unexpected properties. This

work indicates that DSD is a powerful and efficient method that allows optimizing certain processes, even in large-scale experiments and fabrication, with a minimal number of experiments, saving time, material, and money and even avoiding scientific frustration. This work on design-of-experiments in material chemistry can be a reference for further optimization of the fabrication of superconducting or other functional thin films.

AUTHOR INFORMATION

Corresponding Authors

Hannes Rijckaert − *Department of Chemistry, Ghent University, 9000 Ghent, Belgium;* orcid.org/0000-0002-6078-2919; Email: Hannes.Rijckaert@UGent.be

Pablo Cayado − *Institute for Technical Physics, Karlsruhe Institute of Technology, 76344 Eggenstein-Leopoldshafen, Germany;* orcid.org/0000-0003-3703-6122; Email: Pablo.Cayado@kit.edu

Authors

Jens Hänisch − *Institute for Technical Physics, Karlsruhe Institute of Technology, 76344 Eggenstein-Leopoldshafen, Germany*

Jonas Billet − *Department of Chemistry, Ghent University, 9000 Ghent, Belgium*

Manuela Erbe − *Institute for Technical Physics, Karlsruhe Institute of Technology, 76344 Eggenstein-Leopoldshafen, Germany*

Bernhard Holzapfel − *Institute for Technical Physics, Karlsruhe Institute of Technology, 76344 Eggenstein-Leopoldshafen, Germany*

Isabel Van Driessche − *Department of Chemistry, Ghent University, 9000 Ghent, Belgium;* orcid.org/0000-0001-5253-3325

Notes

The authors declare no competing financial interest.

ACKNOWLEDGMENTS

The authors thank Max Sieger (Helmholtz-Zentrum Dresden-Rossendorf) for helpful discussions. The authors acknowledge Jan Hasselmeyer (Department of Chemistry, Ghent University) for creating the TOC figure. H.R. acknowledges FWO Flanders for the travel grant (V425418N). This work was partly financially supported by the European Union Horizon 2020 Marie Curie Actions under the project SynFoNY (H2020/2016-722071).

REFERENCES

(1) Obradors, X.; Puig, T.; Pomar, A.; Sandiumenge, F.; Mestres, N.; Coll, M.; Cavallaro, A.; Romà, N.; Gázquez, J.; González, J. C.; Castaño, O.; Gutierrez, J.; Palau, A.; Zalamova, K.; Morlens, S.; Hassini, A.; Gibert, M.; Ricart, S.; Moretó, J. M.; Piñol, S.; Isfort, D.; Bock, J. Progress towards All-chemical Superconducting $YBa_2Cu_3O_7$-Coated Conductors. *Supercond. Sci. Technol.* **2006**, *19* (3), S13−S26.

(2) Obradors, X.; Puig, T. Coated Conductors for Power Applications: Materials Challenges. *Supercond. Sci. Technol.* **2014**, *27* (4), 044003.

(3) Hilgenkamp, H.; Mannhart, J. Grain Boundaries in High-T_c Superconductors. *Rev. Mod. Phys.* **2002**, *74* (2), 485.

(4) Puig, T.; Gutiérrez, J.; Pomar, A.; Llordés, A.; Gazquez, J.; Ricart, S.; Sandiumenge, F.; Obradors, X. Vortex Pinning in Chemical Solution Nanostructured YBCO Films. *Supercond. Sci. Technol.* **2008**, *21* (3), 034008.

(5) Yamada, Y.; Takahashi, K.; Kobayashi, H.; Konishi, M.; Watanabe, T.; Ibi, A.; Muroga, T.; Miyata, S.; Kato, T.; Hirayama, T.; et al. Epitaxial Nanostructure and Defects Effective for Pinning in $Y(RE)Ba_2Cu_3O_{7-x}$ Coated Conductors. *Appl. Phys. Lett.* **2005**, *87* (13), 132502.

(6) Obradors, X.; Puig, T.; Ricart, S.; Coll, M.; Gazquez, J.; Palau, A.; Granados, X. Growth, Nanostructure and Vortex Pinning in Superconducting $YBa_2Cu_3O_7$ Thin Films Based on Trifluoroacetate Solutions. *Supercond. Sci. Technol.* **2012**, *25* (12), 123001.

(7) Diez Sierra, J.; Lopez-Dominguez, P.; Rijckaert, H.; Rikel, M. O.; Hänisch, J.; Khan, M. Z.; Falter, M.; Bennewitz, J.; Huhtinen, H.; Schäfer, S.; et al. High Critical Current Density and Enhanced Pinning in Superconducting Films of $YBa_2Cu_3O_{7-\delta}$ Nanocomposites with Embedded $BaZrO_3$, $BaHfO_3$, $BaTiO_3$ and $SrZrO_3$ Nanocrystals. *ACS Appl. Nano Mater.* **2020**, *3* (6), 5542−5553.

(8) MacManus-Driscoll, J.; Foltyn, S.; Jia, Q.; Wang, H.; Serquis, A.; Civale, L.; Maiorov, B.; Hawley, M.; Maley, M.; Peterson, D. Strongly Enhanced Current Densities in Superconducting Coated Conductors of $YBa_2Cu_3O_{7\ x}$+$BaZrO_3$. *Nat. Mater.* **2004**, *3* (7), 439−443.

(9) Selvamanickam, V.; Gharahcheshmeh, M. H.; Xu, A.; Zhang, Y.; Galstyan, E. Critical Current Density above 15 MA cm ^{2} at 30 K, 3 T in 2.2 μm Thick Heavily-Doped $(Gd,Y)Ba_2Cu_3O_x$ Superconductor Tapes. *Supercond. Sci. Technol.* **2015**, *28* (7), 072002.

(10) Opherden, L.; Sieger, M.; Pahlke, P.; Hühne, R.; Schultz, L.; Meledin, A.; Van Tendeloo, G.; Nast, R.; Holzapfel, B.; Bianchetti, M.; et al. Large Pinning Forces and Matching Effects in $YBa_2Cu_3O_{7-\delta}$ Thin Films with $Ba_2Y(Nb/Ta)O_6$ Nano-precipitates. *Sci. Rep.* **2016**, *6*, 21188.

(11) Malmivirta, M.; Rijckaert, H.; Paasonen, V.; Huhtinen, H.; Hynninen, T.; Jha, R.; Awana, V. S.; Van Driessche, I.; Paturi, P. Enhanced Flux Pinning in YBCO Multilayer Films with BCO Nanodots and Segmented BZO Nanorods. *Sci. Rep.* **2017**, *7* (1), 1−8.

(12) Rijckaert, H.; Cayado, P.; Nast, R.; Diez Sierra, J.; Erbe, M.; López Dominguez, P.; Hänisch, J.; De Buysser, K.; Holzapfel, B.; Van Driessche, I. Superconducting HfO_2-$YBa_2Cu_3O_{7-\delta}$ Nanocomposite Films Deposited Using Ink-Jet Printing of Colloidal Solutions. *Coatings* **2020**, *10* (1), 17.

(13) De Keukeleere, K.; Cayado, P.; Meledin, A.; Vallès, F.; De Roo, J.; Rijckaert, H.; Pollefeyt, G.; Bruneel, E.; Palau, A.; Coll, M.; Ricart, S.; Van Tendeloo, G.; Puig, T.; Obradors, X.; Van Driessche, I. Superconducting $YBa_2Cu_3O_{7\ \delta}$ Nanocomposites Using Preformed ZrO_2 Nanocrystals: Growth Mechanisms and Vortex Pinning Properties. *Adv. Electr. Mater.* **2016**, *2* (10), 1600161.

(14) Cayado, P.; De Keukeleere, K.; Garzón, A.; Perez-Mirabet, L.; Meledin, A.; De Roo, J.; Vallés, F.; Mundet, B.; Rijckaert, H.; Pollefeyt, G.; Coll, M.; Ricart, S.; Palau, A.; Gazquez, J.; Ros, J.; Van Tendeloo, G.; Van Driessche, I.; Puig, T.; Obradors, X. Epitaxial $YBa_2Cu_3O_{7-x}$ Nanocomposite Thin Films from Colloidal Solutions. *Supercond. Sci. Technol.* **2015**, *28* (12), 124007.

(15) Rijckaert, H.; Hänisch, J.; Pollefeyt, G.; Bäcker, M.; Van Driessche, I. Influence of Ba^{2+} Consumption and Intermediate Dwelling during Processing of $YBa_2Cu_3O_7$ Nanocomposite Films. *J. Am. Ceram. Soc.* **2019**, *102* (7), 3870−3878.

(16) Maier, W. F. The Combinatorial Approach. *Mater. Today* **2004**, *7* (10), 55−56.

(17) von Wenckstern, H.; Zhang, Z.; Schmidt, F.; Lenzner, J.; Hochmuth, H.; Grundmann, M. Continuous Composition Spread using Pulsed-Laser Deposition with a Single Segmented Target. *CrystEngComm* **2013**, *15* (46), 10020−10027.

(18) Feng, Z.; Yuan, J.; Li, J.; Wu, X.; Hu, W.; Shen, B.; Qin, M.; Zhao, L.; Zhu, B.; Stanev, V., High-throughput Investigation of Tunable Superconductivity in FeSe Films. *arXiv* 2018; 1402.3163.

(19) Jung, J.; Yim, H.; Parmar, N. S.; Lee, J.-S.; Choi, J.-W. Continuous Composition Spread and Electrochemical Studies of Low Cobalt Content Li $(Ni,Mn,Co)O_2$ Cathode Materials. *Coatings* **2019**, *9* (6), 366.

(20) Xiao, L.; Lin, D. K.; Bai, F. Constructing Definitive Screening Designs using Conference Matrices. *J. Qual. Technol.* **2012**, *44* (1), 2−8.
(21) Jones, B.; Nachtsheim, C. J. Effective Design-Based Model Selection for Definitive Screening Designs. *Technometrics* **2017**, *59* (3), 319−329.
(22) Billet, J.; Dujardin, W.; De Keukeleere, K.; De Buysser, K.; De Roo, J.; Van Driessche, I. Size Tunable Synthesis and Surface Chemistry of Metastable TiO_2-Bronze Nanocrystals. *Chem. Mater.* **2018**, *30* (13), 4298−4306.
(23) Hayasaka, R.; Cayado, P.; Erbe, M.; Freitag, W.; Hänisch, J.; Holzapfel, B.; Ito, S.; Hashizume, H. Investigation of the Crystallization Process of CSD-ErBCO on IBAD-Substrate via DSD Approach. *Sci. Rep.* **2020**, *10* (1), 1−7.
(24) Obradors, X.; Martínez-Julián, F.; Zalamova, K.; Vlad, V.; Pomar, A.; Palau, A.; Llordés, A.; Chen, H.; Coll, M.; Ricart, S.; et al. Nucleation and Mesostrain Influence on Percolating Critical Currents of Solution Derived $YBa_2Cu_3O_7$ Superconducting Thin Films. *Phys. C* **2012**, *482*, 58−67.
(25) Ternero, P.; Alcalà, J.; Piperno, L.; Pop, C.; Ricart, S.; Mestres, N.; Obradors, X.; Puig, T.; Sotgiu, G.; Celentano, G.; Palau, A. Low-Fluorine Ba-Deficient Solutions for High-Performance Superconducting YBCO Films. *Coatings* **2021**, *11* (2), 199.
(26) Lei, L.; Zhao, G.; Xu, H.; Wu, N.; Chen, Y. Influences of Y_2O_3 Nanoparticle Additions on the Microstructure and Superconductivity of YBCO Films Derived from Low-Fluorine Solution. *Mater. Chem. Phys.* **2011**, *127* (1), 91−94.
(27) Xu, Y.; Shen, M. Structure and Optical Properties of Nanocrystalline $BiFeO_3$ Films Prepared by Chemical Solution Deposition. *Mater. Lett.* **2008**, *62* (20), 3600−3602.
(28) George, J.; Smet, P.; Botterman, J.; Bliznuk, V.; Woestenborghs, W.; Van Thourhout, D.; Neyts, K.; Beeckman, J. Lanthanide-assisted Deposition of Strongly Electro-optic PZT Thin Films on Silicon: Toward Integrated Active Nanophotonic Devices. *ACS Appl. Mater. Interfaces* **2015**, *7* (24), 13350−13359.
(29) Yeo, H. G.; Trolier-McKinstry, S. {001} Oriented Piezoelectric Films Prepared by Chemical Solution Deposition on Ni Foils. *J. Appl. Phys.* **2014**, *116* (1), 014105.
(30) De Keukeleere, K.; Coucke, S.; De Canck, E.; Van Der Voort, P.; Delpech, F.; Coppel, Y.; Hens, Z.; Van Driessche, I.; Owen, J. S.; De Roo, J. Stabilization of Colloidal Ti, Zr, and Hf Oxide Nanocrystals by Protonated Tri-n-octylphosphine Oxide (TOPO) and Its Decomposition Products. *Chem. Mater.* **2017**, *29* (23), 10233−10242.
(31) Rijckaert, H.; De Roo, J.; Van Zele, M.; Banerjee, S.; Huhtinen, H.; Paturi, P.; Bennewitz, J.; Billinge, S.; Bäcker, M.; De Buysser, K.; et al. Pair Distribution Function Analysis of ZrO_2 Nanocrystals and Insights in the Formation of ZrO_2-$YBa_2Cu_3O_7$ Nanocomposites. *Materials* **2018**, *11* (7), 1066.
(32) Huijbregtse, J.; Rector, J.; Dam, B. Effect of the Two (100) $SrTiO_3$ Substrate Terminations on the Nucleation and Growth of $YBa_2Cu_3O_{7-\delta}$ Thin Films. *Phys. C* **2001**, *351* (3), 183−199.
(33) Rijckaert, H.; De Roo, J.; Roeleveld, K.; Pollefeyt, G.; Bennewitz, J.; Bäcker, M.; Lynen, F.; De Keukeleere, K.; Van Driessche, I. Microwave-Assisted $YBa_2Cu_3O_7$ Precursors: A Fast and Reliable Method towards Chemical Precursors for Superconducting Films. *J. Am. Ceram. Soc.* **2017**, *100* (6), 2407−2418.
(34) Lavrakas, P. J. *Encyclopedia of Survey Research Methods*. Sage Publications: 2008.
(35) Rijckaert, H.; Pollefeyt, G.; Sieger, M.; Hänisch, J.; Bennewitz, J.; De Keukeleere, K.; De Roo, J.; Hühne, R.; Bäcker, M.; Paturi, P.; Huhtinen, H.; Hemgesberg, M.; Van Driessche, I. Optimizing Nanocomposites through Nanocrystal Surface Chemistry: Superconducting $YBa_2Cu_3O_7$ Thin Films via Low-Fluorine Metal Organic Deposition and Preformed Metal Oxide Nanocrystals. *Chem. Mater.* **2017**, *29* (14), 6104−6113.
(36) Akaike, H. A New Look at the Statistical Model Identification. *IEEE Trans. Autom. Control* **1974**, *19* (6), 716−723.
(37) Erbe, M.; Cayado, P.; Freitag, W.; Ackermann, K.; Langer, M.; Meledin, A.; Hänisch, J.; Holzapfel, B. Comparative Study of CSD-grown REBCO Films with Different rare Earth Elements: Processing Windows and T_c. *Supercond. Sci. Technol.* **2020**, *33* (9), 094002.
(38) Feenstra, R.; Lindemer, T. B.; Budai, J. D.; Galloway, M. D. Effect of Oxygen Pressure on the Synthesis of $YBa_2Cu_3O_{7-x}$ Thin Films by Post-Deposition Annealing. *J. Appl. Phys.* **1991**, *69* (9), 6569−6585.
(39) Wördenweber, R. Growth of High-T_c Thin Films. *Supercond. Sci. Technol.* **1999**, *12* (6), R86−R102.
(40) Erbe, M.; Hänisch, J.; Hühne, R.; Freudenberg, T.; Kirchner, A.; Molina-Luna, L.; Damm, C.; Van Tendeloo, G.; Kaskel, S.; Schultz, L.; et al. $BaHfO_3$ Artificial Pinning Centres in TFA-MOD-derived YBCO and GdBCO Thin Films. *Supercond. Sci. Technol.* **2015**, *28* (11), 114002.
(41) Doudkowsky, M.; Santiso, J.; Berton, S.; Figueras, A.; Bassas, J. Barium Incorporation in C-axis Oriented YBCO Thin Films Deposited by Metalorganic Chemical Vapour Deposition. *Phys. C* **1997**, *288* (1−2), 1−9.
(42) Vostokov, N. V.; Gaponov, S. V.; Gribkov, B. A.; Drozdov, Y. N.; Masterov, D. V.; Mironov, V. L.; Nozdrin, Y. N.; Pestov, E. E. Effect of Cation Composition on the Superconducting Properties and on the Microstructure of YBaCuO Thin Films. *Phys. Solid State* **2003**, *45* (11), 2025−2030.
(43) Talantsev, E.; Xia, J.; Strickland, N.; Hoffmann, C.; Morgan, S.; Long, N.; Rupich, M.; Li, X.; Sathyamurthy, S. Nucleation And Growth Of Ba-Reduced Metal Organic Deposited YBCO Films. *AIP Conf. Proc.* **2009**, 56−59.
(44) Zhang, H. L.; Ding, F. Z.; Gu, H. W.; Dong, Z. B.; Qu, F.; Shang, H. J. Effect of Ba/Y Molar Ratio on Superconducting Properties of $BaTiO_3$-Doped $YBa_2Cu_3O_{7-\delta}$ Films. *J. Supercond. Novel Magn.* **2016**, *29* (5), 1227−1232.
(45) Chen, H.; Zalamova, K.; Pomar, A.; Granados, X.; Puig, T.; Obradors, X. Growth Rate Control and Solid−Gas Modeling of TFA-$YBa_2Cu_3O_7$ Thin Film Processing. *Supercond. Sci. Technol.* **2010**, *23* (3), 034005.